International Journal of Thermofluids 23 (2024) 100704

Contents lists available at ScienceDirect

International Journal of Thermofluids

journal homepage: www.sciencedirect.com/journal/international-journal-of-thermofluids

Numerical analysis of unsteady free convection under the combined influence of inclined magnetohydrodynamic and exothermic chemical reaction in an enclosure filled with nanofluid

Hussein H. Alaydamee [a], Mohammed Azeez Alomari [b,c,*], Qusay H. Al-Salami [d], Farah Q.A. Alyousuf [e], Faris Alqurashi [f], Mujtaba A. Flayyih [g]

[a] Department of Chemical Engineering, University of Al-Qadisiyah, College of Engineering, Al-Qadisiyah, 58002, Iraq
[b] Department of Mechanical Engineering, University of Al-Qadisiyah, Ad-Diwaniyah, 58001, Iraq
[c] College of Engineering, University of Warith Al-Anbiyaa, Karbala, Iraq
[d] Department of Business Administration, College of Administrative and Financial Sciences, Cihan University-Erbil, Iraq
[e] Department of Computer Network, College of Engineering and Computer Science, Lebanese French University, Erbil, Kurdistan Region, Iraq
[f] Mechanical Engineering Dept., College of Engineering, University of Bisha, Bisha, Saudi Arabia
[g] Biomedical Engineering Department, College of Engineering and Technologies, Al-Mustaqbal University, Hillah, Iraq

ARTICLE INFO

Keywords:
MHD
Unsteady-natural convection
Inclined MHD
Exothermic reaction
Trapezoidal enclosure

ABSTRACT

Unsteady study of the natural convection of aluminum oxide-water nanofluid within a trapezoidal geometry containing a circular cylinder located at its center. Finite Element method has been considered for the numerical analysis. The proposed investigation handled the impact of Rayleigh number (10^3–10^5), chemical reaction parameter (0–4), aluminum oxide nanoparticles volume fraction (0–0.06), magnetic field (0–63) and its inclination angle (0°–90°), and circular obstacle diameter (0.3–0.7) effects on time-dependent natural convection of Al_2O_3–H_2O nanofluid. On the other hand, the value of Prandtl number has kept constant at (Pr = 6.2). Since the nanofluid mobility at $\varphi = 0.02$, Ha = 3, and $F_k = 1$ significantly improved, the heat transfer rate achieved its maximum intensity at Ra = 10^5. Research also reveals a little effect on heat transfer by increasing the fraction of nanoparticles. Additionally, as Ha intensifies from 0 to 63, a final change in the mean Nusselt number of 28.65 % is displayed. Finally, as the magnetic field angle of rotation is diminished, more enhancement in heat transmission is achieved. This research provides insights into the intricate relationship between natural convection and exothermic reaction under the influences of various conditions. This can illustrate the flow and thermal behaviors of nanofluid in such non-uniform shapes in many engineering applications.

1. Introduction

Investigating the nanomaterials' contribution to the enhancement of heat transfer processes can go back to 1995 when Choi and Eastman [1] worked on examining the impacts of nanosolids on the fluid's thermal conductivity. Since then, nanofluids' influences on heat transfer have gained major attention and become one of the attractive fields of study by an enormous number of researchers worldwide [2–11]. Researchers have investigated the intricate relationship of nanoparticles and heat transmission in a wide range of enclosures [12–21], due to their important and abundant field of application in industry [22,23]. The variations of several parameters were taken into account in the investigation of natural convection in an enclosure filled with nanofluids to study their effects on heat transmission and nanofluid velocity. Abdulkadhim et al. [24] reviewed the free convection in complicated cavities under the effects of different governing parameters (Ra, Ha, ϕ, etc.) and the influence of including various shapes of obstacles inside the studied geometries and concluded that the investigation of inner obstacle inside a trapezoidal cavity is limited in the literature. Mojtaba et al. [25] examined recent studies that used nanofluids as the primary parameter to increase buoyancy-driven convection's thermal behavior in a variety of applications such as cooling, heating, and others. The studies are arranged according to the geometry of suggested systems and simulations, which are extensively employed in various applications. In Rehman et al. [26] study, a rectangular cavity containing nanofluid and double-wavy rods as the heat source was examined for internal

* Corresponding author.
E-mail address: mohammed.hasan@qu.edu.iq (M.A. Alomari).

https://doi.org/10.1016/j.ijft.2024.100704

Available online 19 May 2024

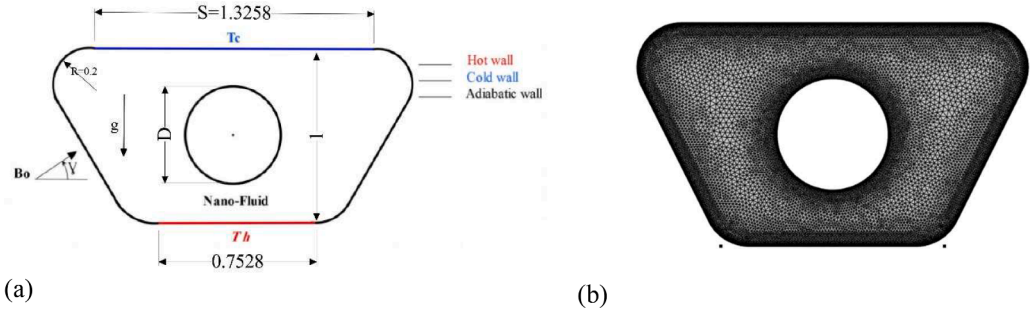

Fig. 1. (a) Schematic view of the studied enclosure, (b) meshing view.

convection. They have tested the variation of Ra number (10^4–10^6), volume fraction of nanoparticles (0.1–0.3), and micropolar number (0–5). Their findings stated that increasing the Rayleigh number and micropolar parameter results in enhancing the thermal flow and found that the Nusselt number is enhanced by augmenting the value of Ra. They also concluded that utilizing higher values of nanoparticle volume fraction produces an obvious impact on heat transfer rate. The natural convection of aluminum oxide/water nanofluid was studied by Nayak et al. [27] inside a hexagonal enclosure containing double diamonds and subjected to the effects of a magnetic field. The lower inclined walls were considered at higher temperatures while the inner obstacles were maintained at lower temperatures leaving the horizontal walls as adiabatic. The results claimed that increasing Ra to 10^6 showed a 76.16 % rise in the Nusselt number. 6.3 % and 7.5 % increase in Nu number occurred when the cold diamonds position changed to the top and bottom of the enclosure respectively, instead of keeping the original position. A rectangular enclosure equipped with nanofluid was considered in Vinodhini and Prasad [28] work for the studies of natural convection performance under the magnetic field application. The acquired findings demonstrate the thermal fields and nanofluid flow in intriguing ways. Raising the Schmidt number causes the cavity center region to compress and lowers the iso-concentration values in the enclosure's central area. The findings indicate that in the presence of a heat source, the local Nusselt number significantly decreases, particularly in the middle region of the surface, while the nearby sections do not significantly alter. Nonetheless, the presence of a heat sink raises the Nusselt number, with the effect being most noticeable near the wall's center. In Hosseinjani and Nikfar [29] numerical investigation, a rhombus enclosure with a lower temperature than higher temperature cylinders was used to test the natural convection performance of Cu/water nanofluid. Their study handled four possible flow cases that may be generated near the cylinders: unstable and asymmetric flow with regular periodic behavior, unsteady and asymmetric flow with non-periodic behavior, and steady and symmetric flow. The results indicate that the symmetric and stable flow is frequently generated for Ra values of 10^4 and 10^5. The results also indicate that, at Ra 10^6, an increase in φ typically results in an improvement in flow stability. Furthermore, the maximum Nu_L number on the cylinder surface grows as the Ra number climbs to 10^6. The local and mean Nu numbers for low Ra values (Ra = 10^4) are not very much a consequence of variations of φ. A numerical simulation of heat transmission in a wavy trapezoidal enclosure with and without the existence magnetic field is included in the Khalil et al. [30] research. They studied the variations of operating parameters such as wave numbers, amplitude, Ra number, and Hartmann number. The results showed an enhancement of 3.16 to 3.37 times in heat transmission and 5–80 times in energy enhancement. The lowest average Nu was found at Ha = 0 and Ra = 5×10^2, along with the greatest value of Tc = 25 °C. The optimal maximum average Nu was found at Ha = 40, Ra = 2.5×10^4, and the smallest value of Tc = 0 °C. Sen et al. [31] research examined a trapezoidal enclosure, filled with aluminum oxide/water nanofluid, that had been heated unevenly. The findings show that although raising the Hartmann number inhibits heat transmission, increasing the Rayleigh number and concentration of nanoparticles facilitates it. The total thermal performance of the trapezoidal cavity is largely influenced by all pertinent elements, with the frequency of the non-uniform heating generally improving it noticeably. Utilizing the finite volume approach, a 3D numerical study of the impact of an applied magnetic field inclination on free convection flow within an open trapezoidal geometry equipped with carbon nanotube nanofluid has been conducted by Al-Sayegh [32]. According to the findings, the heat transmission rate is observed to decrease with increasing Ha at high Rayleigh number values, however, heat transfer is enhanced with increasing solid volume percentage, irrespective of the magnetic field's inclination angle. At 60° inclination angle of the magnetic field, 0.05 vol % of nanoparticles, 25 Hartman number, and 10^5 Ra, the greatest heat transfer rate was observed. The influence of the existence of exothermic reactions has been examined by researchers to study its contribution as a heat source [33–40]. An investigation is conducted by Umavathi and Sheremet [41] to assess the impact of an exothermic chemical reaction on the spontaneous thermo-solutal convection in a horizontal channel containing a permeable nanofluid that is sparsely packed. It is discovered that the system is most unstable at a certain critical Frank–Kamenetskii number. It is discovered that the initiation of convection is delayed as the viscosity ratio increases. Compared to the scenario where chemical reactions don't occur, the fluid in the porous media is more unstable when there are exothermic chemical reactions. Under an applied magnetic field and fully developed continuous free convection flow, Hamza et al. [42] investigated an Arrhenius-driven chemical process in a microchannel. They found that when the governing parameters and chemical reaction are increased, the fluid velocity and volume flow rate increase, respectively, but there is noticeable flow hindering when the Hartman number is increased. Some more studies in different cases can be found in the following papers [43–46]

From the literature review, there is a lack in steadying the unsteady natural convection of nanofluid in a cavity under double influence of inclined MHD and exothermic chemical reaction. The current study enhances the knowledge of heat transfer in chemical vessels. The considered case is a chamfered trapezoidal with internal cylinder with different sizes. Convection changes over time. For the suggested problem, numerical solutions to the partial differential equations are handled using the finite element method. Some important variables have been considered in this steady such as Ra (10^3–10^5), F_k (0–4), ϕ (0–0.06), Ha (0–63), γ (0–90). The study outcomes are presented using mean Nusselt number graphs, temperature isolines, and stream function isolines. The majority of current research indicates that no such study has been discovered to deal with this sort of issue.

1.1. Physical model and validation

This study considers a trapezoidal cavity containing a circular cylinder located at the center of the cavity. The trapezoidal enclosure's bottom horizontal wall is kept at high temperatures while the top one is kept at low temperatures. All other parts of the cavity including the circumference of the circular object and chamfered edges are considered

Table 1
Thermophysical characteristics of water and aluminum oxide nanoparticles at (25 C) Hasan et al. [33].

Properties	κ[$Wm^{-1}K^{-1}$]	μ[$kgm^{-1}s^{-1}$]	β[K^{-1}]	ρ[kgm^{-3}]	cp[$Jkg^{-1}K^{-1}$]	σ[Sm^{-1}]
H_2O	0.613	0.001003	21×10^{-5}	997.1	4179	5.5×10^{-6}
Al_2O_3	40		8.5×10^{-6}	3970	765	2.7×10^{-6}

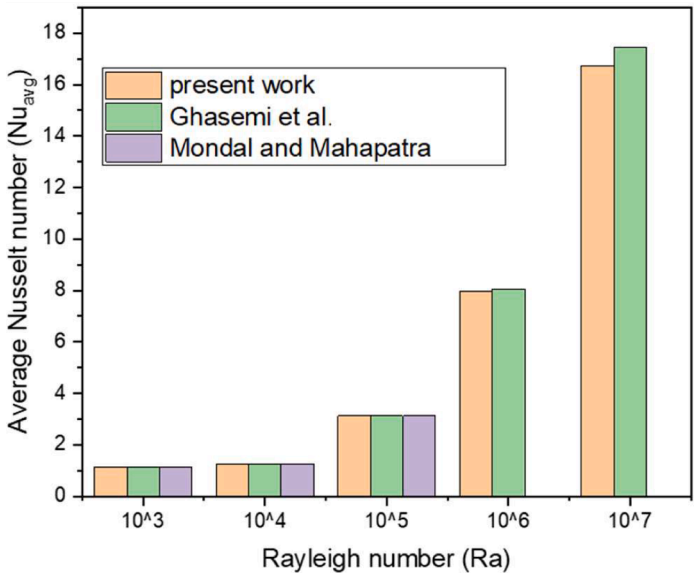

Fig. 2a. Comparing average Nusselt number of the present work with Ghasemi et al. [47] and Mondal and Mahapatra [48].

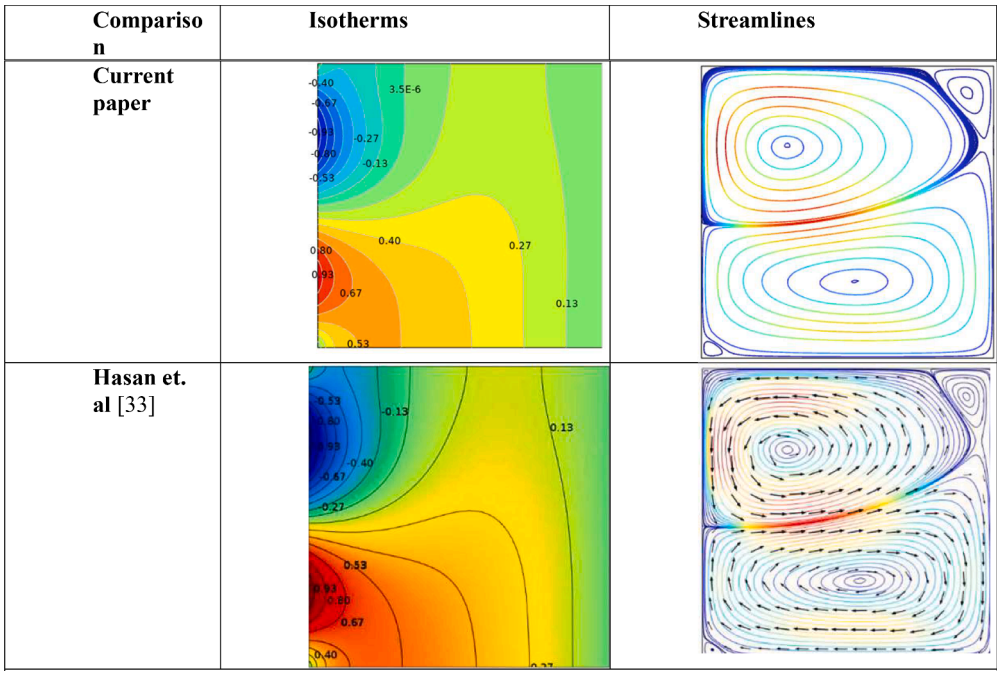

Fig. 2b. Validation of the current problem with Hasan et al. [33] at $\varphi = 0.05$, Ha $= 40$, $F_k = 2$, $\gamma = 0$, Ra $= 10^4$, $T_0 = 25$ and $\tau = 5$ s.

adiabatic. The circular obstacle diameter was investigated for three different cases. In case 1, the diameter of the circular barrier is kept at 0.3, while it is assumed to be 0.5 and 0.7 in case 2 and case 3 respectively. A magnetic field, natural convection, and nanofluid flow have been judged in the geometry. Fig. 1 illustrates the enclosure with the physical description having 0.2 radius chamfered corners. The lower-left corner of the cavity represents the origin of the coordinate. The horizontal and vertical walls are represented by the x-axis and y-axis respectively. Al_2O_3/water nanofluid thermophysical properties in Table 1 are applied in the simulation. Because the postulated problem's solutions are straightforward, the radiation influence is disregarded in this study's application of Arrhenius chemical processes connected to the presence of a magnetic field. Utilizing the hydromagnetic field and its inclination angle, the momentum equations are integrated to

Table 2
Mesh dependency in terms of average Nusselt number precision at $F_k = 2$, Ha = 12, φ = 0.03, Ra = 10^5 (9908 elements used).

No	Number of elements	Mean Nusselt number
1	1385	3.9137
2	2167	3.9148
3	3296	3.9201
4	**9908**	**4.225**
5	26,645	4.222

comprehend heat transfer and flow dynamics when a magnetic field is present. To evaluate the described problem confidently, a validation comparison has been conducted based on previously published work as illustrated in Fig. 2a, b. Performing a precision analysis is crucial to obtaining accurate results; therefore, a mesh dependency is established at $F_k = 2$, Ha = 12, φ = 0.03, and Ra = 10^5 for aluminum oxide/water nanofluid in terms of average Nusselt number as shown in Table 2 where 9908 elements are used for the proposed study.

1.2. Mesh dependent study

The numerical analysis is very sensitive to the number of the elements which consist of the mesh for the considered geometry. Furthermore, the results become more accurate with increasing the number of elements and hence the mesh is usually called fined mesh; however, with the increase of the elements, the time of the analysis becomes longer and the cost becomes higher. For that reason, a mesh-dependent study is carried out to choose the best mesh for the current study with fewer elements and acceptable accuracy. Furthermore, this is only possible by applying local mesh refinement, where the regions with huge physical change, the regions close to the solid surfaces, need higher refinement while the regions away from the solid surfaces require less mesh refinement. The current case has been examined with five different meshes as can be seen in Table 2 which shows the number of elements with the value of the Nu average at Fk = 2, Ha = 12, and Ra = 105. According to the table, the best choice for the current study at mesh 4 which consists from 9908 elements.

1.3. Modeling

This study model takes into account the 2D time/dependent natural convection of aluminum oxide-water nanofluid, identifying nanosolids as the main fluid species, to evaluate the heat transmission and fluid flow behavior in the trapezoidal cavity. The Arrhenius equation, which states that chemical reaction occurs at the first-order rate (assumed to be constant and dependent on the absolute temperature), is used to study the exothermic chemical processes in geometry. Lazarovici et al. [49] states that it may be represented as follows

$$r = k_0 a\, e^{\left(-\frac{E}{RT}\right)} \tag{1}$$

Below are the numerous partial differential equations, including energy, and momentum conservation equations which have been derived depending on the Boussinesq approximation [50,51]

$$\frac{\partial u}{\partial x} + \frac{\partial v}{\partial y} = 0 \tag{2}$$

$$u\frac{\partial u}{\partial x} + v\frac{\partial u}{\partial y} = \frac{\mu_n}{\rho_n}\left(\frac{\partial^2 u}{\partial x^2} + \frac{\partial^2 u}{\partial y^2}\right) - \left(\frac{\partial p}{\rho_n\, \partial x} + \frac{\partial u}{\partial t}\right) - \left[u\, sin^2(\gamma) - v\, sin(\gamma) cos(\gamma)\right] B_0^2 \frac{\sigma_n}{\rho_n} \tag{3}$$

$$u\frac{\partial v}{\partial x} + v\frac{\partial v}{\partial y} = \frac{\mu_n}{\rho_n}\left(\frac{\partial^2 v}{\partial x^2} + \frac{\partial^2 v}{\partial y^2}\right) + g\frac{(\rho\beta)_n}{\rho_n}(T - T_c) - \left(\frac{\partial p}{\rho_n \partial y} + \frac{\partial v}{\partial t}\right) - \left[v\, cos^2(\gamma) - u\, sin(\gamma)\, cos(\gamma)\right] B_0^2 \frac{\sigma_n}{\rho_n} \tag{4}$$

$$u\frac{\partial T}{\partial x} + v\,\frac{\partial T}{\partial y} = \alpha_n\left(\frac{\partial^2 T}{\partial x^2} + \frac{\partial^2 T}{\partial y^2}\right) + \frac{Qk_0\, a}{\rho_n Cp_n\, e^{\frac{E}{RT}}} - \frac{\partial T}{\partial t} \tag{5}$$

The following equations of nanofluid effective density, mass expansion coefficient, thermal diffusivity, and volumetric thermal and heat capacities [52] are written as follows

$$\rho_n = \varphi\rho_p + \rho_b(1-\varphi) \tag{6}$$

$$\rho_n Cp_n = \varphi\rho_p Cp_p + \rho_b Cp_b(1-\varphi) \tag{7}$$

$$\alpha_n = \frac{\kappa_n}{\rho_n Cp_n} \tag{8}$$

$$\rho_n\beta_n = \varphi\rho_p\beta_p + \rho_b\beta_b(1-\varphi) \tag{9}$$

$$\rho_n\beta_n^* = (-\varphi)\left(\rho_b\beta_b^*\right) + \varphi\rho_p\beta_p^* \tag{10}$$

To obtain the nanofluid effective dynamic viscosity, Chandrashekar et al. [53] equation is utilized as follows:

$$\frac{\mu_n}{\mu_b} = \left(\frac{1}{1-\varphi}\right)^{2.5} \tag{11}$$

Bruggeman et al. [54] model is utilized to estimate the nanofluid thermal conductivity as shown below:

$$\kappa_n = 0.25\left[\left(3\varphi\kappa_p - \kappa_p\right) + \left(2\kappa_b - 3\varphi\kappa_b\right)\right] + \frac{\kappa_b}{4}\sqrt{\Delta} \tag{12}$$

Where:

$$\Delta = (3\varphi - 1)^2\left(\frac{\kappa_p}{\kappa_b}\right)^2 + (2 - 3\varphi)^2 + 2\left(\frac{\kappa_p}{\kappa_b}\right)\left(2 + 9\varphi - 9\varphi^2\right) \tag{13}$$

The boundary conditions can be written as follows, knowing that the cavity length is denoted by L, and the temperature of hot surfaces and cold surfaces are denoted by $T_h and T_c respectively$:

$$\frac{\partial T}{\partial y} = 0,\ v = v = 0,\ \forall\, 0 \le x \le L,\ y = L \tag{14}$$

$$\frac{\partial T}{\partial y} = 0,\ v = u = 0,\ \forall\, 0 \le x \le L,\ y = 0 \tag{15}$$

$$T = T_c + (T_h - T_c),\ v = u = 0,\ \forall\, x = 0,\ 0 \le y \le L \tag{16}$$

$$T = T_c,\ v = u = 0,\ \forall\, x = L,\ 0 \le y \le L \tag{17}$$

$$y = LY,\ x = XL,\ v = \frac{V\alpha_b}{L},\ u = \frac{U\alpha_b}{L},\ t = \frac{\tau L^2}{\alpha_b},\ p = \frac{P\alpha_b^2\rho_b}{L^2},\ \theta = \frac{(T - T_0)E}{RT_0^2} \tag{18}$$

dimensionless equations are obtained as follows [50,51]:

$$\frac{\partial U}{\partial X} + \frac{\partial V}{\partial Y} = 0 \tag{19}$$

$$U\frac{\partial U}{\partial X} + V\frac{\partial U}{\partial Y} = \frac{\mu_n}{\rho_n}\left(\frac{\partial^2 U}{\partial X^2} + \frac{\partial^2 U}{\partial Y^2}\right)\frac{Pr}{\nu_b} - \left(\frac{\rho_b \partial P}{\rho_n \partial X} + \frac{\partial U}{\partial \tau}\right) - \left\{U sin^2(\gamma) - V sin(\gamma)\cos(\gamma)\right\} Pr.Ha^2\, \frac{\rho_b\sigma_n}{\rho_n\sigma_b} \tag{20}$$

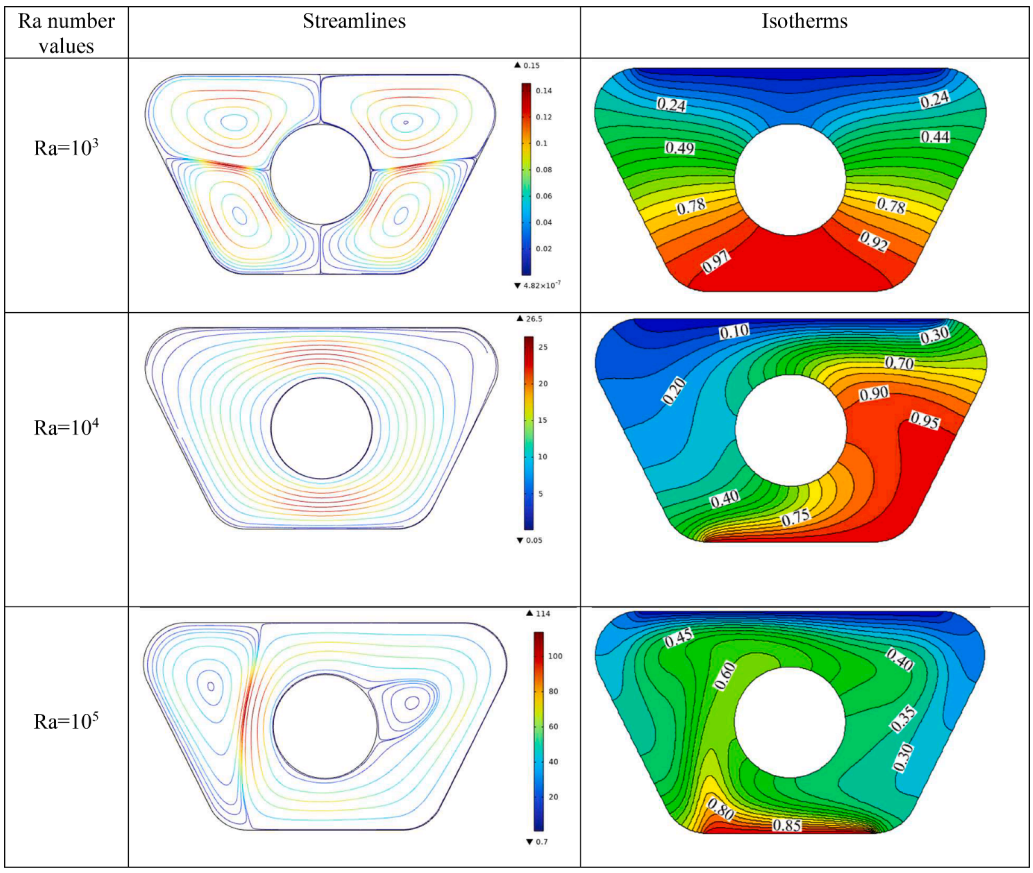

Fig. 3. Rayleigh parameter impact in terms of streamlines and isotherms at φ = 0.02, Ha = 3, F_k = 1, case 2, and time = 5 s.

$$U\frac{\partial V}{\partial X}+V\frac{\partial V}{\partial Y}=\frac{\mu_n}{\rho_n}\left(\frac{\partial^2 V}{\partial X^2}+\frac{\partial^2 V}{\partial Y^2}\right)\frac{Pr}{\nu_b}+\left(\frac{\rho_n\beta_n}{\rho_n\beta_b}\right)\theta.Pr.Ra-\left(\frac{\rho_b\partial P}{\rho_n\partial Y}+\frac{\partial V}{\partial \tau}\right)-Pr.Ha^2\frac{\rho_b\sigma_n}{\rho_n\sigma_b}\left\{Vcos^2(\gamma)-Usin(\gamma)\cos(\gamma)\right\} \tag{21}$$

$$U\frac{\partial \theta}{\partial X}+V\frac{\partial \theta}{\partial Y}=\frac{\alpha_n}{\alpha_b}\left(\frac{\partial^2 \theta}{\partial X^2}+\frac{\partial^2 \theta}{\partial Y^2}\right)+\frac{(\rho_b Cp_b)}{(\rho_n Cp_n)}F_k e^{\theta}-\frac{\partial \theta}{\partial \tau} \tag{22}$$

The governing parameters can be written in the dimensionless form as follows:

The Frank–Kamenetskii number:

$$F_k=\left(\frac{E}{RT_0}\right)\frac{L^2 Qk_0 a}{T_0\kappa_b}e^{-\frac{E}{RT_0}} \tag{23}$$

The Hartmann number:

$$Ha=B_0 L\sqrt{\frac{\sigma_b}{\mu_b}} \tag{24}$$

The Rayleigh number:

$$Ra=\frac{L^3 g\beta_b RT_0^2}{E\alpha_b\nu_b} \tag{25}$$

The Prandtl number:

$$Pr=\frac{\nu_b}{\alpha_b} \tag{26}$$

Dimensionless boundary conditions are written as follows:

$$\frac{\partial \theta}{\partial Y}=0,\ V=U=0,\ \forall\, 0\le Y\le 1,\ X=0 \tag{27}$$

$$\frac{\partial \theta}{\partial Y}=0,\ V=U=0,\ \forall\, 0\le Y\le 1,\ X=1 \tag{28}$$

$$\theta=0,\ V=U=0,\ \forall\, 0\le X\le 1,\ Y=1 \tag{29}$$

$$\theta=1,\ V=U=0,\ \forall\, 0\le X\le 1,\ Y=0 \tag{30}$$

To assess the heat transfer, local and average Nusselt number, and coefficient of heat transfer can be utilized.

$$Nu_L=\frac{Lq}{\kappa_b T_0} \tag{31}$$

Where *qcanbeexpressedasduetotheexistanceofchemicalreaction*:

$$q=-\frac{\kappa_n E}{RT_0}\left(\frac{\partial T}{\partial x}\right)_{x=0} \tag{32}$$

Using Eq. (13), the local Nusselt number can be expressed as follows:

$$Nu_L=-\frac{\partial \theta}{\partial X}\frac{\kappa_n}{\kappa_b} \tag{33}$$

and the average Nusselt number on the cold wall can be expressed as follows [50,51]:

$$Nu_{avg}=-\frac{\kappa_n}{\kappa_b S}\int_0^S\frac{\partial \theta}{\partial X}dY \tag{34}$$

The flow velocity can be written as:

$$R_v=\sqrt{v^2+u^2} \tag{35}$$

The dimensionless velocities U and V are related to the stream function gradient (Ψ) as:

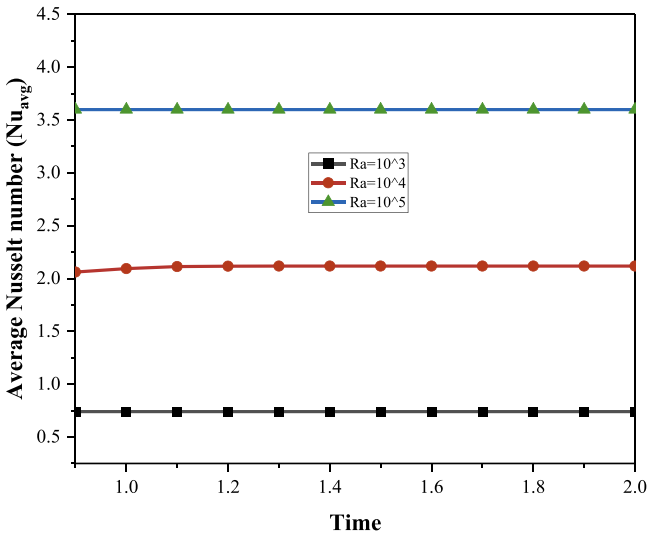

Fig. 4. Mean Nusselt number for different Ra values at φ = 0.03 at $F_k = 0$, Ha = 2, Ra = 10^5.

$$U = \frac{\partial \Psi}{\partial y},\ V = -\frac{\partial \Psi}{\partial x} \tag{36}$$

2. Results and discussion

The numerical investigation utilizing the Finite Element Method is illustrated in terms of nanofluid streamlines, temperature isolines, and the average Nusselt number data. Fig. 3 shows the streamlines and isothermal contours of the proposed centered-circle obstacle of case 2 cavity for various Ra values (10^3, 10^4, and 10^5) where the nanoparticles volume fraction of 0.02, Frank–Kamenetskii number value of 1, Hartman number value of 3, and time of 5 s were all kept unchanged. The nanofluid flow performance of the studied Ra range shows three different regimes. For Ra = 10^3, the existence of the cylinder object in the center of the trapezoidal cavity produces four vortices distributed almost equally with the enclosure around the centered cylinder leaving the nanofluid naturally circulating at a low speed within the four vortices. Increasing the Ra value to 10^4 led to the disappearance of all vortices affected the nanofluid movement to circulate smoothly around the obstacle without the generation of any vortex, reaching a maximum flow velocity of 25. This maximum velocity of the nanofluid was concentrated at the top and bottom parts of the cylinder. Further augmentation of Ra value to 10^5 intensified the velocity of the nanofluid to reach the highest value which is considered four times the maximum velocity value reached for the previous case. The nanofluid movement in

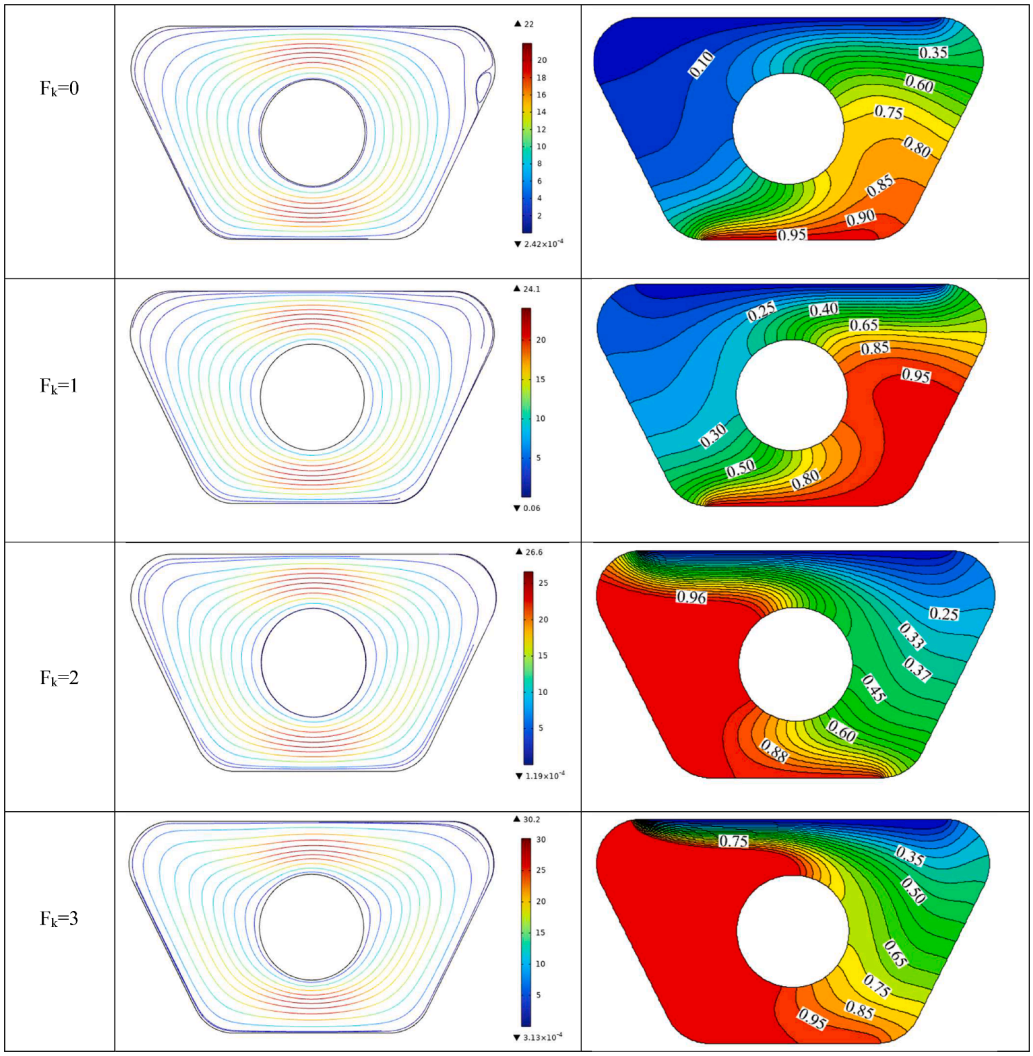

Fig. 5. Frank–Kamenetskii parameter effects in terms of streamlines and isotherms at Ra = 10^4, Ha = 6, φ = 0.04, case 2, time = 5 s.

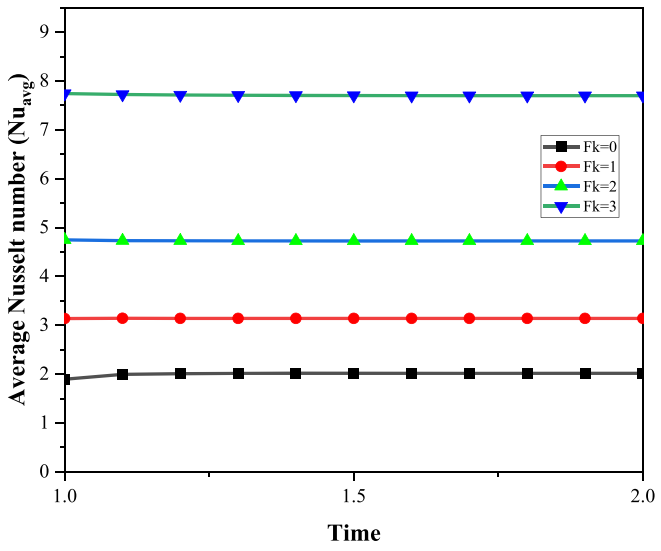

Fig. 6. Mean Nusselt number for different F_k values at Ra = 10^4, Ha = 6, ϕ = 0.04, case 2.

this case was obvious to circulate in the right two-thirds part of the enclosure around the cylindrical object having a small vortex near the top right surface of the centered cylinder. The left one-third part of the cavity noticed a circulation of the nanofluid along the cavity having the maximum velocities at the middle vertical zone where the right two-thirds part and the left one-third part meet.

According to the presented results, the isothermal contours seem to distribute uniformly from the hot bottom wall up toward the center of the enclosure having a smooth transmission around the left and right sides of the obstacle but having a little tendency to transmit farther to the right side. This tendency was intensified by amplifying the value of Ra from 10^3 to 10^4 having a heat transfer in a counterclockwise direction around the cylinder. It is noticeable that heat transmission saw its most optimal intensification at Ra = 10^5 owing to the impressive enhancement of nanofluid movement. The combined effects of buoyancy force and the existence of the obstacle drive the heat to dissipate more effectively upward in a counterclockwise direction. Augmentation of Ra to 10^5 effects on heat transfer agrees with the figures of Nu_{avg}, as illustrated in Fig. 4, showing that when increasing the Ra number, more effective enhancement of the mean Nusselt number is achieved.

Fig. 5 displays the natural convection in terms of isothermal contours and streamlines when varying the Frank–Kamenetskii number in the suggested enclosure after 5 s, with the following parameters held constant: the nanoparticles' volume fraction of 0.04, the Ra = 10^4, the Hartman number value of 6, the diameter of the centered circle obstacle (case 2). It is noticeable that increasing the F_k number from 0 to 3 results in a rise in the nanofluid flow velocity by 36.36 % but does not cause any generation of vortices with the geometry. The effect of F_k number on the heat transmission is of high importance as the results show that when increasing F_k from 0 to 1, the isotherms appear to extend effectively in a counterclockwise direction around the obstacle. However, further intensifying of F_k to 2 changed this trend to extend more rapidly in a clockwise direction around the circle. The intricate relationship between the exothermic reaction, nanofluid buoyancy force, and the presence of a circular obstacle at the center of the geometry is believed to be the reason behind such a trend transition. When F_k is raised to a value of 3, the heat transfer regime becomes higher and more intensified in a similar direction. This phenomenon illustrates that the heat generated is becoming more intensified when there is an exothermic reaction acting as an additional heat source. Fig. 6 explains this trend of F_k number intensification from 0 to 3 in which the average Nusselt number is presented at Ra = 10^4, Ha = 6, and φ = 0.04. The data explained that as F_k augmented to 3, the mean Nusselt number was found to enhance by double the rise achieved when it is intensified to 2.

Keeping the nanoparticles volume fraction of 0.06,

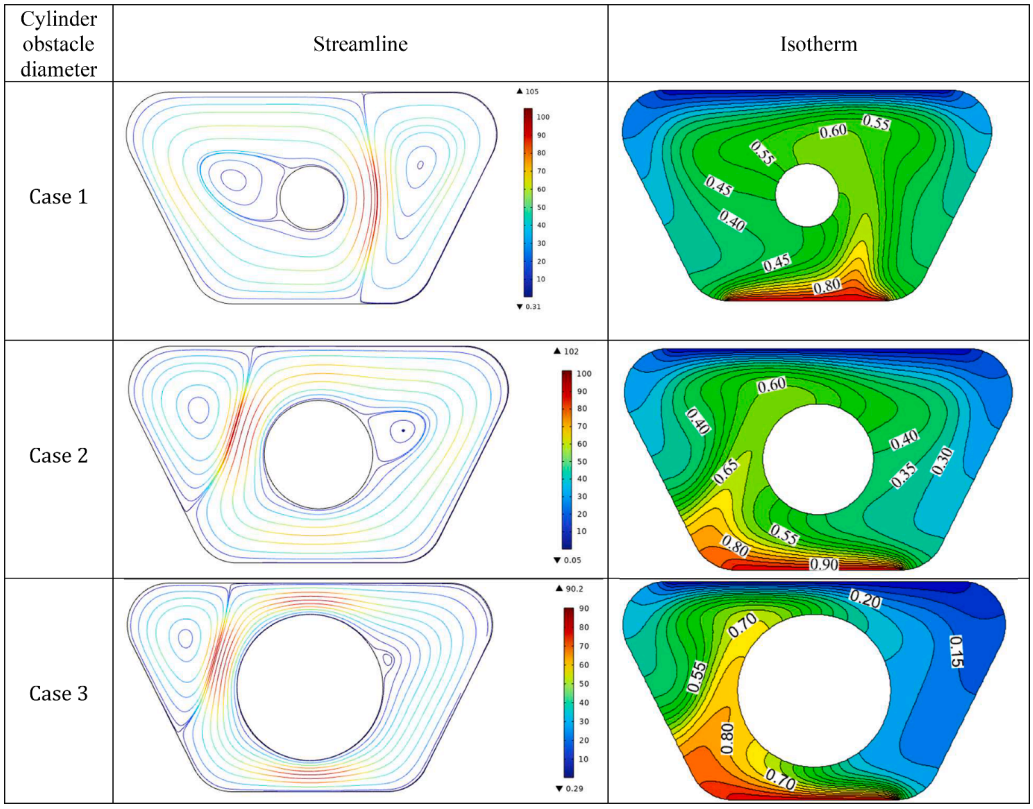

Fig. 7. Obstacle diameter impact in terms of streamlines and isotherms at Ra = 10^5, φ = 0.06, F_k = 1, Ha = 9, time = 5 s.

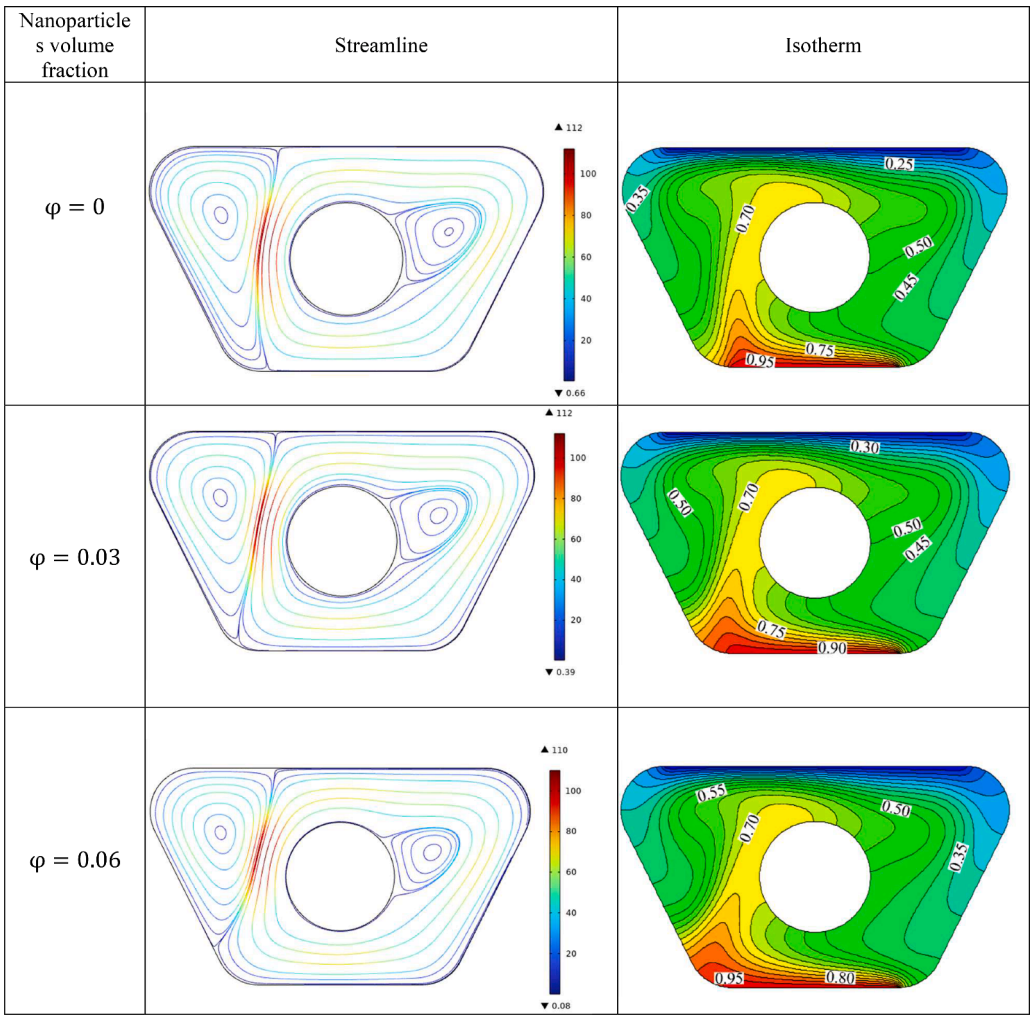

Fig. 8. Aluminum oxide nanoparticles impact in terms of streamlines and isotherms at Ra = 10^5, F_k = 2, Ha = 4, cylinder diameter = 0.3, time =5 s.

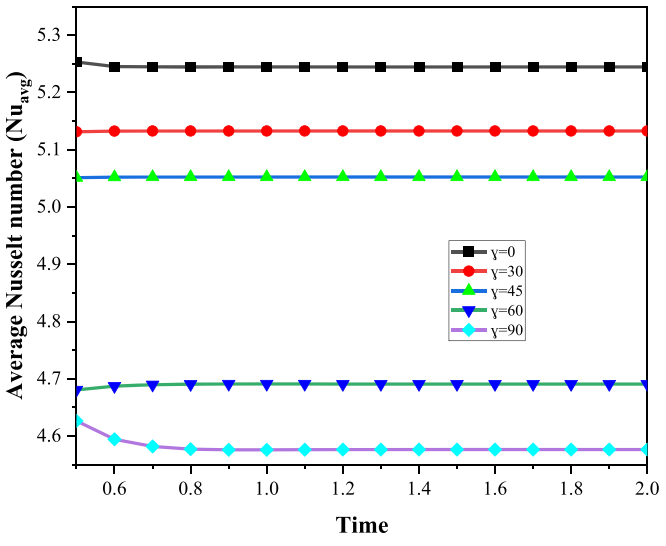

Fig. 9. Mean Nusselt number for various nanoparticles concentration at F_k = 2, Ha = 4, Ra = 10^5.

Frank–Kamenetskii number value of 1, Hartman number value of 9, Ra value of 10^5, and time of 5 s, Fig. 7 displays the influences of changing the diameter of the circle from 0.3 (case 1), 0.5 (case 2), and 0.7 (case 3) on natural convection by showing the nanofluid streamlines and isothermal contours within the trapezoidal cavity. According to the results, when increasing the diameter of the cylinder from 0.3 to 0.7, the streamlines express a slight drop in velocity by 16.66 % since the increase in the cylinder diameter increases the area that hinders the movement of the fluid. As a result, the generated vortices diminish as the circle diameter increases. The figures for the isotherms show that case 1 saw a different trend than that for cases 2 and 3. When increasing the diameter of the circle from 0.3 to 0.5 the fluid tends to move clockwise transferring more heat around the circle while further augmentation of the diameter of the object enhances the clockwise heat transfer allowing for better effective heat exchange within the cavity.

Fig. 8 illustrates the impact of intensifying the nanoparticle volume fraction of nanofluid from 0 to 0.06 for a constant value of all other operating parameters such as Ra = 10^5, F_k = 2, Ha = 4, cylinder diameter = case 2, t = 5 s, while Fig. 9 shows the average Nusselt number for the range of aluminum oxide nanoparticles concentration. It is found that the figures for the streamlines show a slight drop in the maximum velocity of the nanofluid while the isotherms explore a slight enhancement in heat transfer which can be illustrated by the mean Nusselt number data given in Fig. 9 which revealed that increasing volume fraction of nanoparticles from 0 to 0.06 did not enhance heat transmission by more than 5 %.

Fig. 10 explains the influence of applying a magnetic field in the ranges of 0, 18, 45, and 63 on the nanofluid streams and thermal behavior by maintaining the parameters Ra = 10^5,φ = 0.01, F_k = 1,

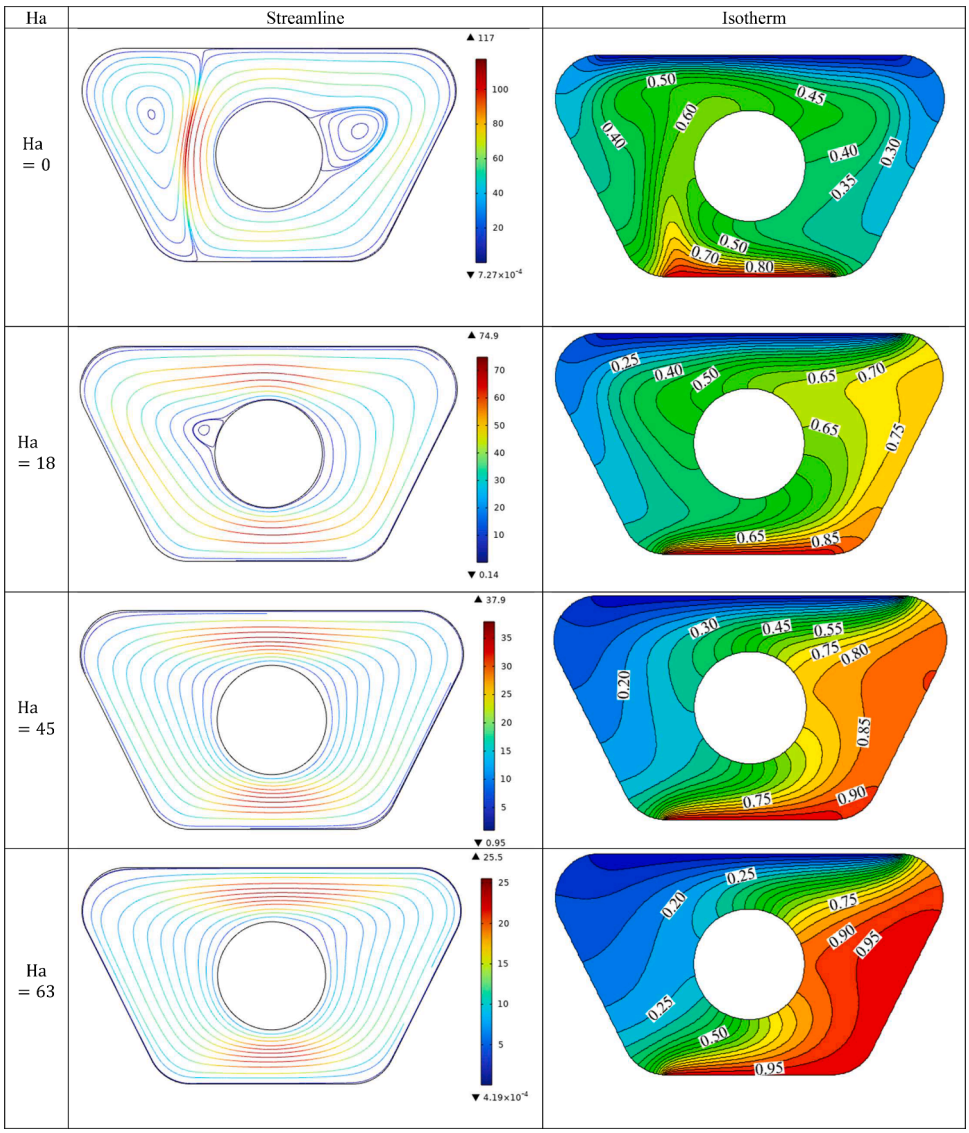

Fig. 10. Hartmann number influence in terms of streamlines and isotherms at Ra = 10^5,φ = 0.01, F_k = 1, cylinder diameter = case 2, time=5 s.

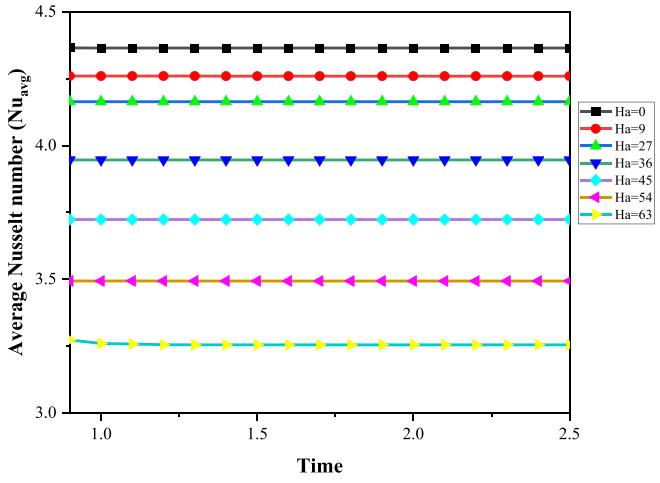

Fig. 11. Mean Nusselt number for different Hartmann numbers at φ = 0.01 at F_k = 1, Ha = 4, Ra = 10^5.

cylinder diameter = 0.3 at a constant value. According to the results, it is found that introducing a magnetic field leads to diminishing the velocity of nanofluid flow thus hindering the heat exchange within the proposed geometry. When increasing the Ha number to 18, 45, and 63, the nanofluid maximum velocity drops by 35.89 %, 67.52 %, and 78.2 % respectively. Thus, as the velocity of the nanofluid becomes less, more heat accumulates near the active bottom wall, the bottom corner, and the right part of the enclosure due to the buoyancy effects. The opposite trend occurs when diminishing the Hartmann number which provides a better enhancement of heat transfer due to the rapid exchange of heat owing to the augmentation of nanofluid flow due to the decrease of Ha number. This can be illustrated in Fig. 11 where the Nusselt number becomes less when the Ha number intensifies from 0 to 63. It is shown that the mean Nusselt number drops by 28.65 % as Ha intensifies from 0 to 63.

To investigate the inclination angle of the supplied magnetic field, various rotational angles were applied such as 0°, 30°, 60°, and 90° keeping constant values of other parameters (F_k = 2, Ra = 10^5, case 2, φ = 0.01). The figures of streamlines saw a drop in nanofluid maximum velocity by 11.52 %, and 22.63 % when raising the angle from 30 to 60 respectively, while the further increase of the angle to 90° led to the opposite trend achieving a rise of 22.84 %. The isothermal contours and

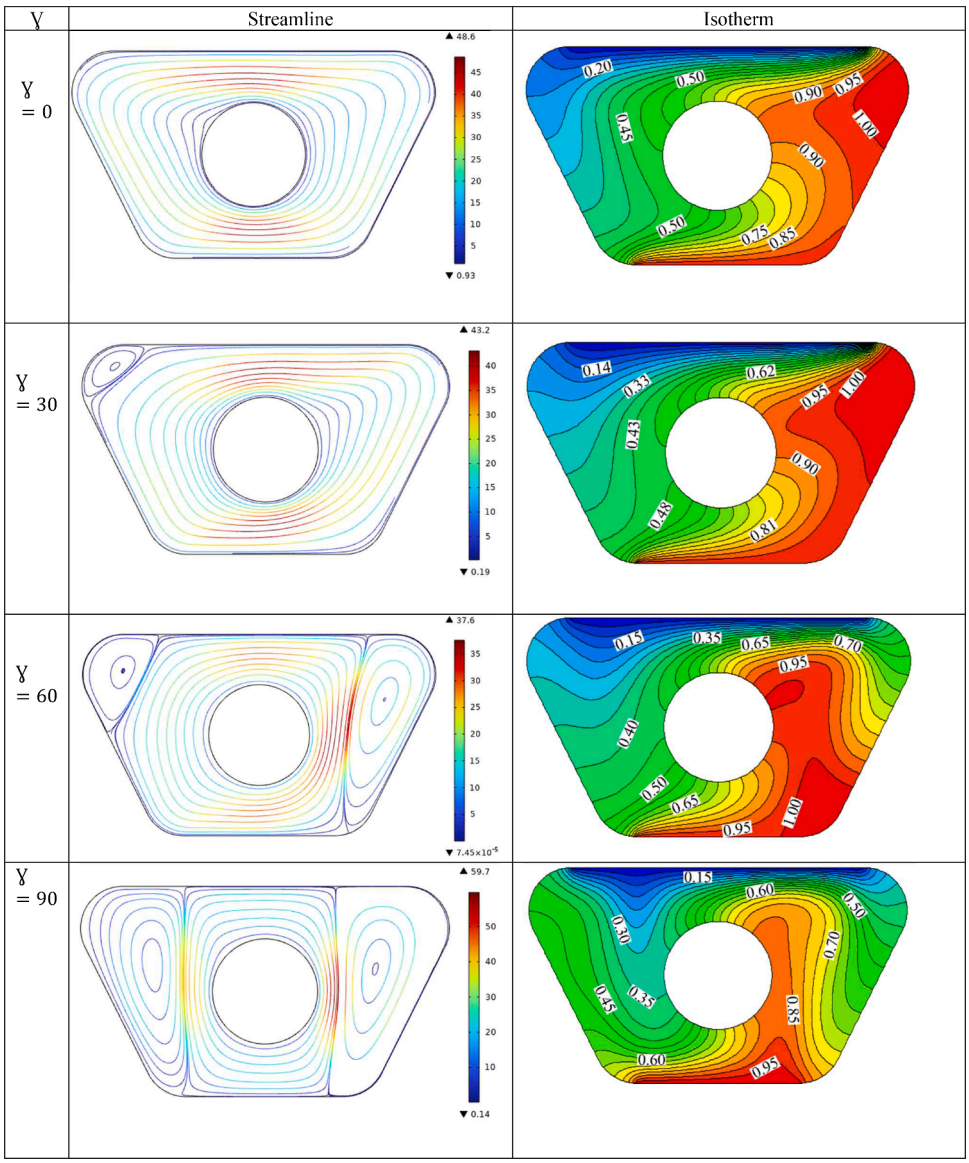

Fig. 12. Magnetic field inclination angle influence in terms of streamlines and isotherms at Ha = 36, F_k = 2, Ra = 10^5, case 2, φ = 0.01, and time =5 s.

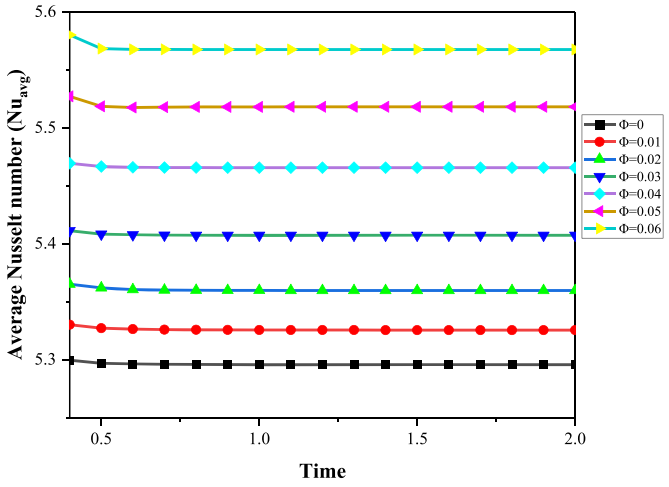

Fig. 13. Mean Nusselt number for various inclination angles of the applied magnetic field at Ha = 36, F_k = 2, Ra = 10^5, and φ = 0.01.

the figures for Nu_{avg} saw impressive outcomes. As the magnetic field angle of rotation is diminished, more enhancement in heat transmission is achieved. It is shown that when there is no rotation, the magnetic field (Ha = 36) achieves the optimum heat transfer enhancement. Figs. 12 and 13 investigate the inclination angle of the supplied magnetic field, various rotational angles were applied such as 0°, 30°, 60°, and 90° keeping constant values of other parameters (F_k = 2, Ra = 10^5, case 2). The figures of streamlines saw a drop in nanofluid maximum velocity by 11.52 %, and 22.63 % when raising the angle from 30 and 60 respectively, while the further increase of the angle to 90° led to the opposite trend achieving a rise of 22.84 %. The isothermal contours and the figures for Nuavg saw impressive outcomes.

3. Conclusion

In conclusion, the proposed investigation handled the impact of Rayleigh number (10^3–10^5), aluminum oxide nanoparticles volume fraction (0–0.06), magnetic field (0–63) and its inclination angle (0°−90°), circular obstacle diameter (0.3–0.7) effects on time-dependent natural convection of Al_2O_3–H_2O nanofluid flow and thermal performance within a trapezoidal shaped enclosure; the results

showed the following impressive insights:

- The heat transmission reached its maximum intensity at Ra = 10^5 because of the remarkable improvement in nanofluid mobility at φ = 0.02, Ha = 3, and F_k = 1. A higher Ra number results in a better enhancement of the mean Nusselt number.
- The flow velocity of the nanofluid rises by 36.36 % when the F_k number is increased from 0 to 3. When F_k increased to 3, the mean Nusselt number was observed to increase by twice as much as when it was heightened to 2 at Ra = 10^4, Ha = 6, and φ = 0.04.
- Results showed that there was no significant increase in heat transfer of more than 5 % when the volume percentage of nanoparticles was increased from 0 to 0.06.
- When the Ha number is raised from 0 to 63, the maximum velocity of the nanofluid decreases by 78.2 %. Furthermore, a 28.65 % drop in the mean Nusselt number is shown as Ha intensifies from 0 to 63.
- It is shown that when there is no rotation, the magnetic field (Ha = 36) achieves the optimum heat transfer enhancement for F_k = 2, Ra = 10^5, and φ = 0.01.

CRediT authorship contribution statement

Hussein H. Alaydamee: Writing – original draft. **Mohammed Azeez Alomari:** Supervision, Software. **Qusay H. Al-Salami:** Formal analysis. **Farah Q.A. Alyousuf:** Formal analysis. **Faris Alqurashi:** Supervision. **Mujtaba A. Flayyih:** Formal analysis.

Declaration of competing interest

The authors declare that they have no known competing financial interests or personal relationships that could have appeared to influence the work reported in this paper.

Data availability

Data will be made available on request.

References

[1] S. Choi, J. Eastman, Enhancing thermal conductivity of fluids with nanoparticles, Am. Soc. Mech. Eng. Fluids Eng. Div. FED 231 (1995) 99–105.

[2] Q.R. Al-Amir, et al., Investigation of natural convection and entropy generation in a porous titled Z-staggered cavity saturated by TiO2-water nanofluid, Int. J. Thermofluids 19 (2023) 100395, https://doi.org/10.1016/j.ijft.2023.100395. June.

[3] B.P. Geridonmez, H.F. Oztop, MHD natural convection in a cavity in the presence of cross partial magnetic fields and Al2O3-water nanofluid, Comput. Math. Appl. 80 (12) (2020) 2796–2810, https://doi.org/10.1016/j.camwa.2020.10.003.

[4] R. Kodi, et al., Influence of MHD mixed convection flow for maxwell nanofluid through a vertical cone with porous material in the existence of variable heat conductivity and diffusion, Case Stud. Therm. Eng. 44 (2023) 102875, https://doi.org/10.1016/j.csite.2023.102875 no. January.

[5] M. Hemmat Esfe, M. Bahiraei, H. Hajbarati, M. Valadkhani, A comprehensive review on convective heat transfer of nanofluids in porous media: energy-related and thermohydraulic characteristics, Appl. Therm. Eng. 178 (2020) 115487, https://doi.org/10.1016/j.applthermaleng.2020.115487.

[6] F. Selimefendigil, H.F. Öztop, MHD natural convection and entropy generation in a nanofluid-filled cavity with a conductive partition. Exergetic, Energetic and Environmental Dimensions, 2018, pp. 763–778.

[7] M.A. Mansour, S. Siddiqa, R.S.R. Gorla, A.M. Rashad, Effects of heat source and sink on entropy generation and MHD natural convection of Al2O3-Cu/water hybrid nanofluid filled with square porous cavity, Therm. Sci. Eng. Prog. 6 (2018) 57–71, https://doi.org/10.1016/j.tsep.2017.10.014.

[8] A.M. Rashad, T. Armaghani, A.J. Chamkha, M.A. Mansour, Entropy generation and MHD natural convection of a nanofluid in an inclined square porous cavity: effects of a heat sink and source size and location, Chinese J. Phys. 56 (1) (2018) 193–211, https://doi.org/10.1016/j.cjph.2017.11.026.

[9] H.R. Ashorynejad, A. Shahriari, MHD natural convection of hybrid nanofluid in an open wavy cavity, Results Phys. 9 (2018) 440–455, https://doi.org/10.1016/j.rinp.2018.02.045.

[10] A. Mourad, et al., MHD natural convection of Fe3O4- MWCNT/Water hybrid nanofluid filled in a porous annulus between a circular cylinder and Koch snowflake, Alexandria Eng. J. 65 (2023) 367–382, https://doi.org/10.1016/j.aej.2022.09.035.

[11] L. Yang, J. Xu, K. Du, X. Zhang, Recent developments on viscosity and thermal conductivity of nanofluids, Powder Technol. 317 (2017) 348–369, https://doi.org/10.1016/j.powtec.2017.04.061.

[12] F.A. Hamad, E. Egelle, S. Gooneratne, P. Russell, Investigation of the effect of aspect ratio on heat transfer from a heated vertical wall to phase change material in a rectangular enclosure, Therm. Sci. Eng. Prog. 42 (2023) 101865, https://doi.org/10.1016/j.tsep.2023.101865 p.

[13] O. Çiçek, M.A. Sheremet, A.C. Baytaş, Effect of natural convection hybrid nanofluid flow on the migration and deposition of MWCNT-Fe3O4 in a square enclosure, Int. J. Therm. Sci. 190 (2023) 108318, https://doi.org/10.1016/j.ijthermalsci.2023.108318 p.

[14] E. Mosheva, I. Krasnyakov, Diffusive–layered convection in Y-shaped continuous-flow microreactor, Exp. Therm. Fluid Sci. 151 (2024) 111100, https://doi.org/10.1016/j.expthermflusci.2023.111100 p.

[15] D. Das, M. Roy, T. Basak, Studies on natural convection within enclosures of various (non-square) shapes – a review, Int. J. Heat Mass Transf. 106 (2017) 356–406, https://doi.org/10.1016/j.ijheatmasstransfer.2016.08.034.

[16] R. Sarlak, A.M. Abed, O.A. Akbari, A. Marzban, S. Baghaei, M. Bayat, Numerical investigation of natural convection heat transfer of water/SWCNT nanofluid flow in a triangular cavity with cold fluid injection, Prog. Nucl. Energy 155 (2023) 104513, https://doi.org/10.1016/j.pnucene.2022.104513.

[17] A. Alazzam, N.A.A. Qasem, A. Aissa, M.S. Abid, K. Guedri, O. Younis, Natural convection characteristics of nano-encapsulated phase change materials in a rectangular wavy enclosure with heating element and under an external magnetic field, J. Energy Storage 57 (2023) 106213, https://doi.org/10.1016/j.est.2022.106213.

[18] S.M. Mirabedin, F. Farhadi, Natural convection in circular enclosures heated from below for various central angles, Case Stud. Therm. Eng. 8 (2016) 322–329, https://doi.org/10.1016/j.csite.2016.08.007.

[19] M.K. Nayak, N. Karimi, A.J. Chamkha, A. Sattar Dogonchi, S. El-Sapa, A.M. Galal, Efficacy of diverse structures of wavy baffles on heat transfer amplification of double-diffusive natural convection inside a C-shaped enclosure filled with hybrid nanofluid, Sustain. Energy Technol. Assess. 52 (2022) 102180, https://doi.org/10.1016/j.seta.2022.102180.

[20] A. Fattahi, N. Hajialigol, M. Delpisheh, N. Karimi, Lattice-Boltzmann numerical simulation of double-diffusive natural convection and entropy generation in an n-shaped partially heated storage tank, Eng. Anal. Bound. Elem. 146 (2023) 105–118, https://doi.org/10.1016/j.enganabound.2022.10.007.

[21] A. Rahimi, M. Sepehr, M.J. Lariche, M. Mesbah, A. Kasaeipoor, E.H. Malekshah, Analysis of natural convection in nanofluid-filled H-shaped cavity by entropy generation and heatline visualization using lattice Boltzmann method, Phys. E Low-dimensional Syst. Nanostruct. 97 (2018) 347–362, https://doi.org/10.1016/j.physe.2017.12.003.

[22] O. Mahian, et al., Recent advances in modeling and simulation of nanofluid flows-part I: fundamentals and theory, Phys. Rep. 790 (2019) 1–48, https://doi.org/10.1016/j.physrep.2018.11.004.

[23] K.H. Solangi, et al., A comprehensive review of thermo-physical properties and convective heat transfer to nanofluids, Energy 89 (2015) 1065–1086, https://doi.org/10.1016/j.energy.2015.06.105.

[24] A. Abdulkadhim, I. mejbel Abed, N. mahjoub Said, An exhaustive review on natural convection within complex enclosures: influence of various parameters, Chinese J. Phys. 74 (2021) 365–388, https://doi.org/10.1016/j.cjph.2021.10.012.

[25] J. B. T.-M. for S. Mojtaba Tabarhoseini, M. Sheikholeslami, Chapter 2 - Natural convection heat transfer enhancement using nanofluids, in: S.J. Vijay, B. Solomon, A.H.T.S. Meyer (Eds.), Woodhead Publishing Series in Energy, Woodhead Publishing, 2023, pp. 39–62. J. B. T.-M. for.

[26] K.U. Rehman, A.U. Khan, S. Abbas, W. Shatanawi, Thermal analysis of micropolar nanofluid in partially heated rectangular enclosure rooted with wavy heated rods, Case Stud. Therm. Eng. 42 (2023) 102701, https://doi.org/10.1016/j.csite.2023.102701. September 2022.

[27] M.K. Nayak, A.S. Dogonchi, A. Rahbari, Free convection of Al2O3-water nanofluid inside a hexagonal-shaped enclosure with cold diamond-shaped obstacles and periodic magnetic field, Case Stud. Therm. Eng. 50 (2023) 103429, https://doi.org/10.1016/j.csite.2023.103429 no. August.

[28] N. Vinodhini, V.R. Prasad, Numerical study of MAGNETO convective Buongiorno nanofluid flow in a rectangular enclosure under oblique magnetic field with heat generation/absorption and complex wall conditions, Heliyon 9 (7) (2023) e17669, https://doi.org/10.1016/j.heliyon.2023.e17669.

[29] A.A. Hosseinjani, M. Nikfar, Numerical analysis of unsteady natural convection from two heated cylinders inside a rhombus enclosure filled with Cu-water nanofluid, Int. Commun. Heat Mass Transf. 113 (2020) 104510, https://doi.org/10.1016/j.icheatmasstransfer.2020.104510.

[30] W.H. Khalil, I.D.J. Azzawi, A. Al-damook, The optimisation of MHD free convection inside porous trapezoidal cavity with the wavy bottom wall using response surface method, Int. Commun. Heat Mass Transf. 134 (2022) 106035, https://doi.org/10.1016/j.icheatmasstransfer.2022.106035.

[31] N. Sen, S. Nag, H.T. Bamboowala, N.K. Manna, N. Biswas, D.K. Mandal, Magnetohydrodynamic thermal behavior of nanofluid flow in a trapezoidal cavity subjected to non-uniform heating, Mater. Today Proc. 63 (2022) 320–327, https://doi.org/10.1016/j.matpr.2022.03.144.

[32] R. Al-Sayegh, Influence of external magnetic field inclination on three-dimensional buoyancy-driven convection in an open trapezoidal cavity filled with CNT-Water nanofluid, Int. J. Mech. Sci. 148 (2018) 756–765, https://doi.org/10.1016/j.ijmecsci.2018.09.032.

[33] M. Hasan, M.J. Uddin, R. Nasrin, Exothermic chemical reaction of magneto-convective nanofluid flow in a square cavity, Int. J. Thermofluids 16 (2022) 100236, https://doi.org/10.1016/j.ijft.2022.100236 no. October,.
[34] M.M. Rahman, I. Pop, M.Z. Saghir, Steady free convection flow within a titled nanofluid saturated porous cavity in the presence of a sloping magnetic field energized by an exothermic chemical reaction administered by Arrhenius kinetics, Int. J. Heat Mass Transf. 129 (2019) 198–211, https://doi.org/10.1016/j.ijheatmasstransfer.2018.09.105.
[35] A.N. Campbell, S.S.S. Cardoso, A.N. Hayhurst, A comparison of measured temperatures with those calculated numerically and analytically for an exothermic chemical reaction inside a spherical batch reactor with natural convection, Chem. Eng. Sci. 62 (11) (2007) 3068–3082, https://doi.org/10.1016/j.ces.2007.03.008.
[36] Z. Hussain, A.S. Alshomrani, T. Muhammad, M.S. Anwar, Entropy analysis in mixed convective flow of hybrid nanofluid subject to melting heat and chemical reactions, Case Stud. Therm. Eng. 34 (2022) 101972, https://doi.org/10.1016/j.csite.2022.101972.
[37] R.V.M.S.S. Kiran Kumar, P. Durga Prasad, S.V.K. Varma, Analytical study of heat and mass transfer enhancement in free convection flow with chemical reaction and constant heat source in nanofluids, Procedia Eng. 127 (2015) 978–985, https://doi.org/10.1016/j.proeng.2015.11.446.
[38] P. Sreedevi, P.S. Reddy, A.J. Chamkha, Heat and mass transfer analysis of nanofluid over linear and non-linear stretching surfaces with thermal radiation and chemical reaction, Powder Technol. 315 (2017) 194–204, https://doi.org/10.1016/j.powtec.2017.03.059.
[39] P.S. Reddy, P. Sreedevi, A.J. Chamkha, MHD boundary layer flow, heat and mass transfer analysis over a rotating disk through porous medium saturated by Cu-water and Ag-water nanofluid with chemical reaction, Powder Technol. 307 (2017) 46–55, https://doi.org/10.1016/j.powtec.2016.11.017.
[40] A.N. Campbell, S.S.S. Cardoso, A.N. Hayhurst, A comparison of measured temperatures with those calculated numerically and analytically for an exothermic chemical reaction inside a spherical batch reactor with natural convection, Chem. Eng. Sci. 62 (11) (2007) 3068–3082, https://doi.org/10.1016/j.ces.2007.03.008.
[41] J.C. Umavathi, M.A. Sheremet, Chemical reaction influence on nanofluid flow in a porous layer: stability analysis, Int. Commun. Heat Mass Transf. 138 (2022) 106353, https://doi.org/10.1016/j.icheatmasstransfer.2022.106353.
[42] M.M. Hamza, G. Ojemeri, S.K. kwai Ahmad, Insights into an analytical simulation of a natural convection flow controlled by Arrhenius kinetics in a micro-channel, Heliyon 9 (7) (2023) e17628, https://doi.org/10.1016/j.heliyon.2023.e17628.
[43] A. Dogonchi, T. Armaghani, A. Chamkha, D. domiri ganji, Natural convection analysis in a cavity with an inclined elliptical heater subject to shape factor of nanoparticles and magnetic field, Arab. J. Sci. Eng. 44 (2019), https://doi.org/10.1007/s13369-019-03956-x. Jun.
[44] M. Hashemi-Tilehnoee, A. Dogonchi, S.M. Seyyedi, A. Chamkha, D. domiri ganji, Magnetohydrodynamic natural convection and entropy generation analyses inside a nanofluid-filled incinerator-shaped porous cavity with wavy heater block, J. Therm. Anal. Calorim. 141 (2020), https://doi.org/10.1007/s10973-019-09220-6. Jan.
[45] T. Tayebi, A. Chamkha, Magnetohydrodynamic natural convection heat transfer of hybrid nanofluid in a square enclosure in the presence of a wavy circular conductive cylinder, J. Therm. Sci. Eng. Appl. 12 (2020) 31009, https://doi.org/10.1115/1.4044857. Jun.
[46] T. Tayebi, H. Öztop, A. Chamkha, Natural convection and entropy production in hybrid nanofluid filled-annular elliptical cavity with internal heat generation or absorption, Therm. Sci. Eng. Prog. 19 (2020) 100605, https://doi.org/10.1016/j.tsep.2020.100605. Jun.
[47] B. Ghasemi, S. Aminossadati, A. Raisi, Magnetic field effect on natural convection in a nanofluid-filled square enclosure, Int. J. Therm. Sci. 50 (2011) 1748–1756, https://doi.org/10.1016/j.ijthermalsci.2011.04.010. Sep.
[48] P. Mondal, T.R. Mahapatra, MHD double-diffusive mixed convection and entropy generation of nanofluid in a trapezoidal cavity, Int. J. Mech. Sci. 208 (2021) 106665, https://doi.org/10.1016/j.ijmecsci.2021.106665. Jul.
[49] A. Lazarovici, V. Volpert, J.H. Merkin, Steady states, oscillations and heat explosion in a combustion problem with convection, Eur. J. Mech. - B/Fluids 24 (2) (2005) 189–203, https://doi.org/10.1016/j.euromechflu.2004.06.007.
[50] M.M. Hamza, A. Shuaibu, A. Kamba, Unsteady MHD free convection flow of an exothermic fluid in a convectively heated vertical channel filled with porous medium, Sci. Rep. 12 (2022) 11989, https://doi.org/10.1038/s41598-022-16064-y. Jul.
[51] M.M. Hasan, M.J. Uddin, R. Nasrin, Exothermic chemical reaction of magneto-convective nanofluid flow in a square cavity, Int. J. Thermofluids 16 (2022) 100236, https://doi.org/10.1016/j.ijft.2022.100236.
[52] T. Islam, R. Nasrin. Thermal operation by nanofluids with various aspects: a comprehensive numerical appraisal, *Waves Random Complex Media,* 2022, pp. 1–30, https://doi.org/10.1080/17455030.2022.2117430.
[53] J. Chandrashekar, et al., The cells and peripheral representation of sodium taste in mice, Nature 464 (7286) (2010) 297–301, https://doi.org/10.1038/nature08783.
[54] D.A.G. Bruggeman, Berechnung verschiedener physikalischer Konstanten von heterogenen Substanzen. I. Dielektrizitätskonstanten und Leitfähigkeiten der Mischkörper aus isotropen Substanzen, Ann. Phys. 416 (7) (1935) 636–664, https://doi.org/10.1002/andp.19354160705. Jan.